Environmental Pollution 257 (2020) 113610

Contents lists available at ScienceDirect

Environmental Pollution

journal homepage: www.elsevier.com/locate/envpol

Heterogeneous activation of peroxymonosulfate by a biochar-supported Co_3O_4 composite for efficient degradation of chloramphenicols☆

Hengduo Xu [a, b, c, d], Yuechao Zhang [a, e], Jiajia Li [a, e], Qinqin Hao [a, e], Xin Li [a, e], Fanghua Liu [a, b, c, *]

[a] Key Laboratory of Coastal Biology and Utilization, Yantai Institute of Coastal Zone Research, Chinese Academy of Sciences, Yantai, Shandong 264003, PR China
[b] Laboratory for Marine Biology and Biotechnology, Pilot National Laboratory for Marine Science and Technology (Qingdao), Qingdao, 266237, PR China
[c] Center for Ocean Mega-Science, Chinese Academy of Sciences, 7 Nanhai Road, Qingdao, 266071, PR China
[d] Jiangsu Key Laboratory of Anaerobic Biotechnology (Jiangnan University), Wuxi, 214122, PR China
[e] University of Chinese Academy of Sciences, Beijing, 100049, China

ARTICLE INFO

Article history:
Received 26 June 2019
Received in revised form
24 October 2019
Accepted 10 November 2019
Available online 14 November 2019

Keywords:
Co_3O_4-BC
Peroxymonosulfate
Chloramphenicols
Sulfate radical

ABSTRACT

Herein, a new peroxymonosulfate (PMS) activation system was established using a biochar (BC)-supported Co_3O_4 composite (Co_3O_4-BC) as a catalyst to enhance chloramphenicols degradation. The effects of the amount of Co_3O_4 load on the BC, Co_3O_4-BC amount, PMS dose and solution pH on the degradation of chloramphenicol (CAP) were investigated. The results showed that the BC support could well disperse Co_3O_4 particles. The degradation of CAP (30 mg/L) was enhanced in the Co_3O_4-BC/PMS system with the apparent degradation rate constant increased to 5.1, 19.4 and 7.2 times of that in the Co_3O_4/PMS, BC/PMS and PMS-alone control systems, respectively. Nearly complete removal of CAP was achieved in the Co_3O_4-BC/PMS system under the optimum conditions of 10 wt% Co_3O_4 loading on BC, 0.2 g/L Co_3O_4-BC, 10 mM PMS and pH 7 within 10 min. The Co_3O_4/BC composites had a synergistic effect on the catalytic activity possibly because the conducting BC promoted electron transfer between the Co species and HSO_5^- and thus accelerated the Co^{3+}/Co^{2+}redox cycle. Additionally, over 85.0 ± 1.5% of CAP was still removed in the 10th run. Although both $SO_4^{\bullet-}$ and $OH^{\bullet}$ were identified as the main active species, $SO_4^{\bullet-}$ played a dominant role in CAP degradation. In addition, two other chloramphenicols, i.e., florfenicol (FF) and thiamphenicol (TAP), were also effectively degraded with percentages of 86.4 ± 1.3% and 71.8 ± 1.0%, respectively. This study provides a promising catalyst Co_3O_4-BC to activate PMS for efficient and persistent antibiotics degradation.

1. Introduction

Chloramphenicols, as broad-spectrum antibiotics with good antibacterial activity, have been widely used to treat bacterial infections in animal productions (Butler et al., 2016). As a consequence of the high consumption of these antibiotics, they are inevitably discharged into the environment, where they may pose a health risk to humans due to their hematotoxicity, embryotoxicity and potential genotoxicity (Guo et al., 2017). Moreover, the presence of chloramphenicols in the environment ultimately leads to the formation of antibiotic resistant genes that are also considered as pollutants (Li et al., 2013). Although the use of chloramphenicols in food-producing animals in North America and European Union member countries has been severely restricted, they are still being used in developing nations due to their low production cost (Deng et al., 2017a; Liang et al., 2013). However, chloramphenicols cannot be effectively degraded by conventional wastewater treatment plants (WWTPs) and thus end up in environments (Dong et al., 2017; Du et al., 2019). Recently, chloramphenicols have been frequently detected in the environmental waters of China (Li et al., 2016). Therefore, establishing an efficient method to remove

☆ This paper has been recommended for acceptance by Dr. Yong Sik Ok.

* Corresponding author. Yantai Institute of Coastal Zone Research, Chinese Academy of Sciences, Yantai, Shandong, 264003, China.
E-mail address: fhliu@yic.ac.cn (F. Liu).

https://doi.org/10.1016/j.envpol.2019.113610
0269-7491/

chloramphenicols from wastewater is urgently needed.

Recently, advanced oxidation processes (AOPs) based on the generation of sulfate radical ($SO_4^{\bullet-}$) have been proven to be effective in degrading antibiotics (Mahdi-Ahmed and Chiron, 2014). Compared to hydroxyl radicals (OH•) produced from the Fenton process, $SO_4^{\bullet-}$ exhibited a higher standard reduction potential (2.5−3.1 V), more selectivity and independence from pH (Feng et al., 2016; Qi et al., 2018). $SO_4^{\bullet-}$ is formed through electron transfer by transition metal activation of peroxymonosulfate (PMS, HSO_5^-). Co^{2+} based catalysts such as Co_3O_4 are considered the most efficient in PMS activation for $SO_4^{\bullet-}$ generation (Anipsitakis et al., 2006). Co_3O_4 exhibits potential advantages in PMS heterogeneous activation for antibiotics degradation due to its high efficiency over a wide pH range, low dosage, high stability and reusability (Chen et al., 2008). For example, Deng et al. (2017b) reported that chloramphenicol (CAP) was almost completely removed by a Co_3O_4/PMS system at neutral pH. Nevertheless, Co^{2+} leaching from Co_3O_4 is frequently observed, which may lead to secondary pollution in treated water. Furthermore, cobalt loss decreases the catalytic efficiency of Co_3O_4 for PMS activation. To overcome these drawbacks, many attempts to anchor Co_3O_4 onto supporting materials have been reported and shown promising outcomes (Yang et al., 2008; Yang et al., 2019).

Biochar (BC) is a carbonaceous material produced from the pyrolysis of carbon-rich biomass. Its porous structure makes BC a promising support that is easily accessible to metal and metal oxide particles, and that would increase their surface-to-volume ratio and thus promote their catalytic activity for PMS activation (Yan et al., 2015). For example, compared to zerovalent iron, BC supported zerovalent iron showed enhanced activity toward activation of PMS for the degradation of bisphenol A (Jiang et al., 2019). Previous studies have demonstrated that carbon-based materials used as supports can not only reduce Co^{2+} leaching from Co_3O_4, but also facilitate surface Co-OH complex formation, which is considered the critical step in PMS activation (Yao et al., 2012). Additionally, the persistent free radicals in BC can react with PMS to produce $SO_4^{\bullet-}$ and OH• (Jiang et al., 2019). Thus, BC-supported Co_3O_4 may have great potential in activating PMS for chloramphenicols removal, and this ability needs to be evaluated.

In this study, a BC supported Co_3O_4 composite (Co_3O_4-BC) was synthesized and used as catalysts to activate PMS for chloramphenicols removal. Three chloramphenicols, i.e., CAP, florfenicol (FF) and thiamphenicol (TAP), were selected and studied in this study. First, the morphology and structure of Co_3O_4-BC were characterized using scanning electron microscope (SEM) and transmission electronic microscope (TEM). Second, the oxidation performance of the Co_3O_4-BC/PMS system toward chloramphenicols was examined. The catalytic activity of Co_3O_4-BC for PMS activation was characterized using linear sweep voltammetry (LSV), chronoamperometry (CA) and electrochemical impedance spectroscopy (EIS). The effects of the Co_3O_4-BC amount, PMS dose and pH on the removal of chloramphenicols were also examined. Third, the radicals present in the system were identified by electron spin resonance (ESR) and quenching tests. Finally, the reusability of the Co_3O_4-BC catalyst was examined.

2. Materials and methods

2.1. Chemical and materials

$Co(NO_3)_2$•$6H_2O$ and NH_3•H_2O were purchased from Sinopharm Chemical Reagent Co. (Shanghai, China). CAP, TAP, FF and PMS (Oxone, $HSO_5 \cdot 0.5KHSO_4 \cdot 0.5K_2SO_4$, 4.7% active oxygen) were purchased from Sigma-Aldrich (purity>99%). BC was produced from the pyrolysis of wheat straw (Sanli New Energy Co., China). All the reagents used in this study were at least of analytical grade.

2.2. Synthesis of the Co_3O_4-BC composite

The Co_3O_4-BC composite was prepared with a modified coprecipitation method according to the procedure previously reported by Xie et al. (2018). Briefly, 2.0 g of $Co(NO_3)_2$•$6H_2O$ was dissolved in 100 mL of pure water. Additionally, 20 g of BC powder was added to 200 mL of pure water and placed in an ultrasonic bath for 1 h to completely disperse the BC. Then, the $Co(NO_3)_2$ solution was gradually added to the BC dispersion with magnetic stirring. The pH value of the resulting mixed solution was adjusted to ≥9.0 by adding NH_3•H_2O (>25 wt%). After reacting for 12 h and centrifugation, the precipitate was washed with pure water repeatedly to obtain a suspension with a pH value of 7.0. The resulting precipitate was dried at 70 °C for 6 h and calcined in air at 450 °C for 4 h. Then, the Co_3O_4-BC composite was obtained. The loading amount of Co_3O_4 in the composite was 10 wt%. Co_3O_4-BC composites with different loading amounts of Co_3O_4 (5 wt% and 20 wt%) were also synthesized as controls.

2.3. Characterization of the Co_3O_4-BC composite

The morphological information and elemental composition of Co_3O_4-BC were obtained using a field-emission scanning electron microscope (SEM, S4800, Hitachi Co., Japan) equipped with an energy dispersive spectrometer (EDS) (Thermo Fisher Inc., USA). The size distribution of Co_3O_4-BC was observed by a transmission electron microscope (TEM, JEM-1400, JEOL Co., Japan). The metal states on the surface of Co_3O_4-BC were determined by an X-ray photoelectron spectroscopy (XPS) (ESCALAB 250Xi, Thermo Fisher Inc., USA). X-ray diffraction (XRD, X′ Pert PRO MPD, Nederland) patterns of the samples were obtained using an X′ Pert PRO MPD Trax theta-theta diffractometer (Philips Co., Nederland) equipped with Cu Kα radiation. Fourier transform infra-red spectra (FTIR) were recorded on Thermo Fisher Nicolet iS 10 FTIR system. The BET surface area of the Co_3O_4-BC and Co_3O_4 was determined using a surface area and pore size distribution analyzer (Micromeritics ASAP 2460). The electrochemical experiments were carried out using a CHI660 electrochemical workstation (Chenhua, China) with a traditional three-electrode system. The working electrode was a glassy carbon (GC) electrode that was coated with the Co_3O_4-BC composite using a Nafion solution (5 wt%) as the binder and carbon black as the supporting layer. A Ag/AgCl electrode served as the reference electrode, and a Pt thin film electrode acted as the counter electrode. The GC electrode was pretreated by polishing and rinsing prior to use. LSV was performed in a 50 mM phosphate buffer solution (PBS, pH = 7.0) containing 10 mM PMS at a scanning rate of 25 mV/s from 1 to −2 V. CA was performed by applying a constant potential of −0.6 V in PBS with consecutive injection of PMS. EIS was conducted over a frequency range from 0.01 Hz to 100 kHz at −0.6 V with a perturbation signal of 5 mV in PBS containing PMS.

2.4. Experimental procedures

The degradation experiments were conducted in 250 mL conical flasks with magnetic stirring at 26 ± 2 °C. Reactions were initiated by adding PMS (2−15 mM) into 10 mM PBS with pH values ranging from 3 to 11 containing the Co_3O_4-BC catalysts (0.05−0.8 g/L). The initial concentrations of the three chloramphenicols were 30 mg/L. Aqueous samples were withdrawn at different time intervals and then immediately added with excessive sodium thiosulfate before analysis. For comparative purposes, chloramphenicols degradation in Co_3O_4/PMS, BC/PMS and PMS alone systems was conducted as

controls. The quenching agents methanol (MeOH) and tert-butyl alcohol (TBA) were used to explore the oxidation mechanism. All of the above experiments were conducted in triplicate.

2.5. Analytical methods

The concentration of antibiotics over time was determined with a high-performance liquid chromatography (HPLC, 1260 Infinity, Agilent Co., USA) with a photo-diode array detector. For CAP analysis, the mobile phase was methanol and water (65:35) at a wavelength of 275 nm. FF and TAP were analyzed with a mobile phase of methanol-water (40:60) (v/v) at a wavelength of 225 nm. The flow rate of the mobile phase was set as 1 mL/min. Total organic carbon (TOC) was measured using a TOC-VCPH analyzer (Shimadzu Co., Japan). Electron spin resonance (ESR) spectrometry was performed using a JES-FA200 ESR spectrometer. 5,5-Dimethyl-1-pyrrolidine N-oxide (DMPO) was used as a spin-trapping agent for $SO_4^{\bullet -}$ and OH•. Radicals detection was conducted in 50 mM PBS.

3. Results and discussion

3.1. Characterization of the Co_3O_4-BC composite

XRD patterns of BC, Co_3O_4 and Co_3O_4-BC are presented in Fig. 1(a). For BC, the diffraction peaks at 2θ of 21.0° and 26.8° were attributed to the presence of SiO_2, and the peaks at 2θ of 28.2°, 29.6°, 39.7° and 41.8° were attributed to the presence of $CaCO_3$ (Yuan et al., 2011). Co_3O_4 shows a cubic spinel phase with peaks at 2θ = 19.5°, 31.6°, 37.16°, 38.9°, 45.1°, 55.8°, 59.7° and 65.6°, which can be indexed to the known cubic Co_3O_4 phase (JCPDS 42-1647). Two peaks for Co_3O_4-BC were observed at 2θ of 31.5° and 36.8°, which can be assigned to the (220) and (311) planes, respectively, of Co_3O_4. Other characteristic Co peaks were not found, probably due to the low loading amount and high dispersion of Co_3O_4 (Xie et al., 2018).

The atomic composition and elemental valence states of Co_3O_4-BC were confirmed by XPS analysis. The full XPS spectra of Co_3O_4-BC and Co_3O_4 show that the main elements in Co_3O_4-BC are Co, O, C and Si and that Co_3O_4 contains only Co and O (Fig. 1(b)). The Si in the Co_3O_4-BC is ascribed to SiO_2, which was also proven by XRD analysis. The two sharp characteristic peaks for Co_3O_4-BC that appeared at 781.3 and 796.3 eV are ascribed to Co $2p_{3/2}$ and Co $2p_{1/2}$, respectively (Fig. 1(c)), confirming the presence of spinel Co_3O_4. The Co 2p spectra were deconvoluted into four peaks at 781.1, 782.9, 796.2 and 799.5 eV. The peaks at 782.9 and 799.5 eV can be ascribed to Co^{2+}, and the peaks at 781.1 and 796.2 eV can be assigned to Co^{3+} (Deng et al., 2017b). The O 1s XPS spectra can be deconvoluted into two peaks at 530.9 and 533.2 eV, which are assigned to lattice oxygen (O_{latt}) and adsorbed oxygen (O_{ads}), respectively (Fig. 1(d)) (Bai et al., 2013). The O_{ads} will be transferred to $CoOH^+$, which is regarded as the rate-limiting step for PMS activation (Hu et al., 2017a). Compared to the spectrum of Co_3O_4, the spectrum of Co_3O_4-BC exhibited almost no chemical shift. However, the intensity of the Co peak in Co_3O_4-BC was weaker than that in Co_3O_4 due to the low loading amount of Co_3O_4 on the surface of BC, which is consistent with the XRD analysis. In addition, the functional groups of Co_3O_4-BC were also analyzed by FTIR (Fig. S1). The peak at 1020 cm^{-1} was assigned to straight chain C-C stretching (Yuan et al., 2011).

The morphological information of the Co_3O_4-BC composite was determined by SEM and TEM. As shown in Fig. S2(a), BC had a texture structure that endowed it with a large specific surface area, which favored the anchoring of Co_3O_4. The BET surface area of Co_3O_4-BC and Co_3O_4 was 76.4 and 10.8 m^2/g, respectively. The dark portion in the TEM image of the BC was attributed to carbon particle electron scattering (Fig. S2(b)) (Essandoh et al., 2015). Fig. S2 (c) shows that Co_3O_4 has a spherical morphology with an average diameter of 40 nm; however, these Co_3O_4 particles underwent

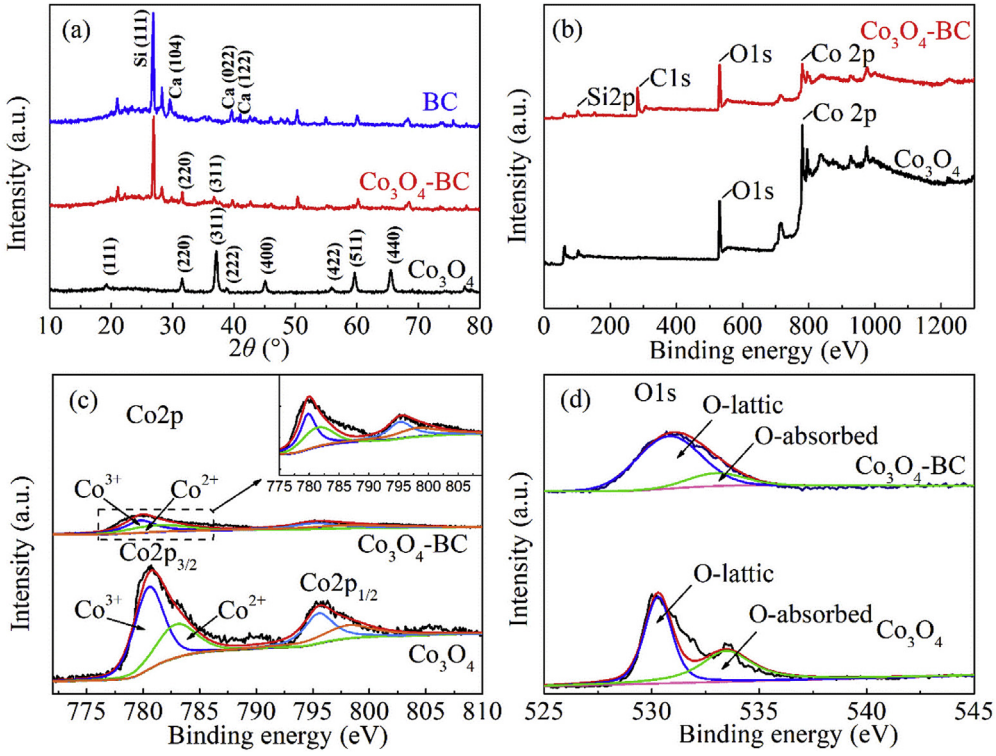

Fig. 1. XRD patterns of BC, Co_3O_4 and Co_3O_4-BC (a) and XPS full scan spectra (b), Co 2p XPS spectra (c) and O 1s XPS spectra (d) of Co_3O_4 and Co_3O_4-BC.

some agglomeration, which is in agreement with the TEM observations (Fig. S2 (d)). It is clearly observed that the Co_3O_4 particles were dispersed uniformly on the surface of BC (Fig. S2 (e)) and that the size of Co_3O_4 was less than 40 nm according to the TEM image of the Co_3O_4-BC composite (Fig. S2 (f)). Multi-elemental EDS mapping images of Co, C and O in the Co_3O_4-BC composite are shown in Fig. S3. The bright spots evidenced a homogeneous distribution of Co in the field of view of the cross-section. In addition, the EDS results show that cobalt, carbon, oxygen, silicon, aluminum and magnesium are present in the Co_3O_4-BC composite (Fig. S4). These results further confirmed the presence of Co_3O_4 in the Co_3O_4-BC composite.

3.2. Electrochemical behaviors of Co_3O_4-BC for PMS activation

Electrochemical techniques including LSV, CA and EIS were performed to characterize the improved catalytic activity of Co_3O_4-BC for PMS activation. The current increased for both Co_3O_4-BC and Co_3O_4 with the addition of PMS (Fig. 2(a)). However, for Co_3O_4-BC, the current was increased immediately after adding PMS at an earlier stage of the CA experiment, meaning that PMS was quickly transformed to $SO_4^{\bullet-}$. The maximum current density of Co_3O_4-BC was 1.76 mA/cm^2, which was higher than that of 1.21 mA/cm^2 for Co_3O_4. In addition, the LSV results also showed that the Co_3O_4-BC electrode had a higher current density than the Co_3O_4 electrode (Fig. 2(b)). These results suggested that the electrons transferred more easily from Co_3O_4-BC to PMS than those from Co_3O_4 and that Co_3O_4-BC possessed superior catalytic activity toward PMS activation. This improved catalytic activity is possibly because conducting BC lowered the electron transfer resistance between Co_3O_4-BC and PMS, which was further suggested by the EIS results in the following discussion.

Nyquist plots express impedance with a real part and an imaginary part as a semicircle (Fig. 2(c)). The impedance at the high frequency limit is the ohmic resistance, which is affected by the electrode materials (He and Mansfeld, 2009). The ohmic resistance of Co_3O_4-BC (11.2 Ω) is lower than that of Co_3O_4 (21.2 Ω), indicating that BC reduced the ohmic resistance. The diameter of the semicircle is the charge transfer resistance. The charge transfer of Co_3O_4-BC is 328.8 Ω, which is much lower than that of Co_3O_4 (2218.2 Ω), suggesting a faster electron transfer rate between Co_3O_4-BC and PMS. These results indicated that compared to BC and Co_3O_4, Co_3O_4-BC possessed superior catalytic activity for PMS activation.

3.3. Chloramphenicols degradation in the Co_3O_4-BC/PMS system

Three chloramphenicols, including CAP, TAP and FF, were selected as the target contaminants to investigate the catalytic oxidation properties of the Co_3O_4-BC/PMS system. These three chloramphenicols were effectively degraded in the Co_3O_4-BC/PMS system with 10 mM PMS and 0.4 g/L Co_3O_4-BC, with degradation percentages of 97.6 ± 1.2%, 71.8 ± 1.0% and 86.4 ± 1.3% for CAP, TAP and FF, respectively (Fig. 3(a)). This is because chloramphenicols with hydroxyl groups usually have low ionization potential values and tend to be easily oxidized by $SO_4^{\bullet-}$ (Hu et al., 2017b; Luo et al., 2017). The chloramphenicols degradation process was described by the pseudo-first order kinetics equation:

$$\ln\left(\frac{C}{C_0}\right) = -k_{app}t \quad (1)$$

where C_0 is the initial concentration of chloramphenicols, C is the chloramphenicols concentration at time t, and k_{app} is the apparent rate constant.

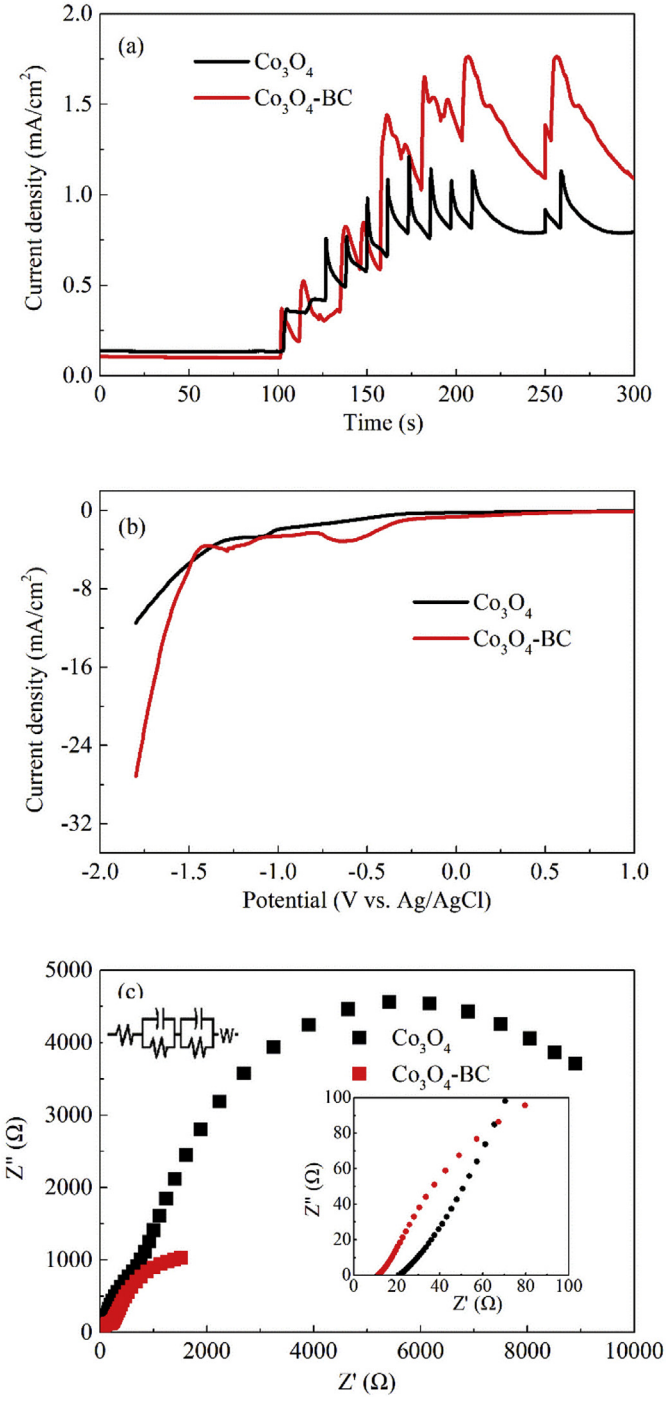

Fig. 2. CA curves (a), LSV curves (b) and Nyquist plot (c) of Co_3O_4 and Co_3O_4-BC. Experimental conditions: [Co_3O_4] = 0.3 g/cm^2, [Co_3O_4-BC] = 0.3 g/cm^2 pH = 7.0 (50 mM phosphate buffer) for (a); [PMS] = 10 mM, pH = 7.0 (50 mM phosphate buffer) for (b) and (c).

The k_{app} values of CAP, TAP and FF were 0.3361, 0.1151 and 0.1793 min^{-1}, respectively. These results suggested that CAP was preferentially degraded over the other two chloramphenicols in the Co_3O_4-BC/PMS system. This selective catalytic oxidation by the Co_3O_4-BC/PMS system was significantly influenced by the physicochemical properties and substituents of the chloramphenicols (Li et al., 2018; Zhang et al., 2019). In addition, the TOC decreased by 45.2 ± 2.0%, 33.9 ± 2.5% and 20.3 ± 1.6% for CAP, TAP and FF, respectively (Fig. S5). In the following experiments, CAP was

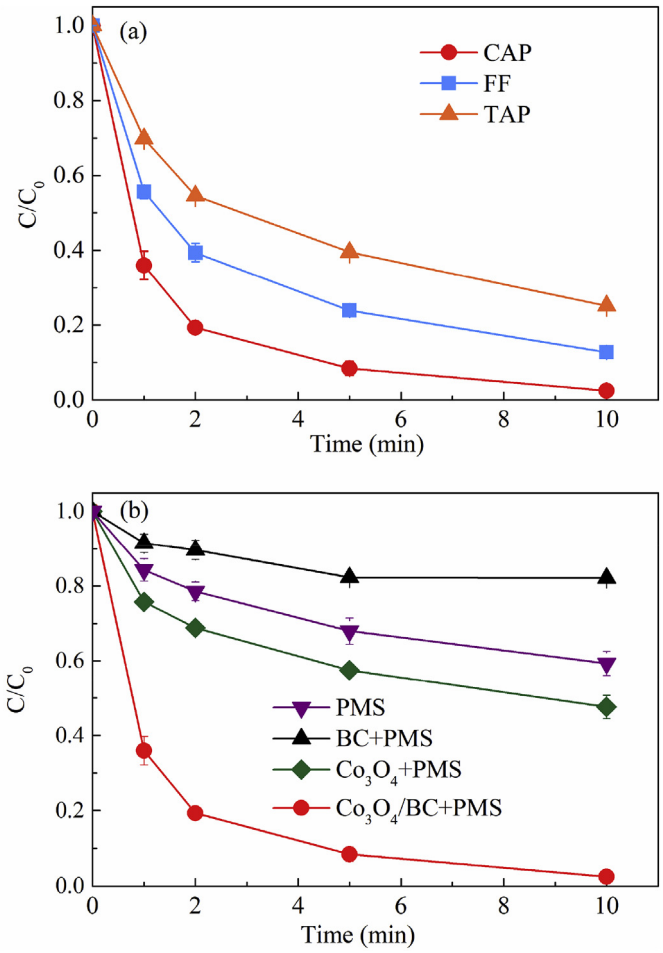

Fig. 3. Degradation of CAP, TAP and FF in the Co_3O_4-BC/PMS system (a), and comparison of CAP degradation by BC-, Co_3O_4- and Co_3O_4-BC-activated PMS and PMS alone. Experimental conditions: [PMS] = 10 mM, [CAP] = 30 mg/L, [TAP] = 30 mg/L, [FF] = 30 mg/L, [Co_3O_4-BC] = 0.2 g/L, [BC] = 0.2 g/L, [Co_3O_4] = 0.2 g/L, pH = 7.0 (50 mM phosphate buffer).

studied as a target chloramphenicols to investigate the degradation performance and mechanism of the Co_3O_4-BC/PMS system because the reactivity of CAP with different reactive species is well-documented.

For comparative purposes, CAP degradation in the Co_3O_4/PMS, BC/PMS and PMS-alone systems was also investigated. As shown in Fig. 3(b), for the pure Co_3O_4 catalyst, 45.4 ± 3.2% of CAP was degraded within 10 min. For the pure BC, the degradation of CAP reached 17.9 ± 0.1% in 10 min, indicating that pure BC is catalytically active possibly because BC contains functional groups such as semiquinone (Wang and Wang, 2019). In addition, several control experiments were conducted and showed that no significant adsorption of CAP on either BC or Co_3O_4-BC surfaces occurred (Fig. S6). In comparation, the degradation of CAP in the Co_3O_4-BC/PMS system was remarkably improved with a removal percentage of 97.6 ± 1.2% under the same conditions, indicating the higher efficiency of PMS activation by Co_3O_4-BC than by pure Co_3O_4 and BC. Furthermore, the degradation efficiency remained at a considerable level even at high concentrations of CAP in the Co_3O_4-BC/PMS system (Fig. S7). However, only approximately 35.5 ± 3.2% of CAP was degraded in the PMS-alone system. It has been reported that unactivated PMS could directly react with organic compounds via nonradical pathways, but this direct reaction was highly dependent on the solution pH and ionic strength (Yang et al., 2018). The k_{app} value of CAP in the Co_3O_4-BC/PMS system was 0.3361 min^{-1}, which was 5.1, 7.2 and 19.4 times greater than the value in the Co_3O_4/PMS (0.0664 min^{-1}), PMS-alone (0.0467 min^{-1}) and BC/PMS (0.0173 min^{-1}) systems, respectively. Similar results were also obtained for the TOC removal rates. The k_{TOC} values of CAP were 0.0523, 0.0252, 0.0085 and 0.0217 min^{-1} in the Co_3O_4-BC/PMS, Co_3O_4/PMS, BC/PMS and PMS-alone systems, respectively (Fig. S8).

Although BC exhibited a limited ability for PMS activation, it acted as a supporting material that significantly promoted the catalytic activity of Co_3O_4. This synergistic effect is possibly because (1) BC provides a large surface area for the dispersal of Co_3O_4 nanoparticles, which can prevent the agglomeration of Co_3O_4 nanoparticles into large particles and obstruct the facile loss of catalytic activity, and (2) the BC with a unique electronic structure and fast electron migration property may accelerate electron transfer between surface CoO and Co_2O_3, which is beneficial for $SO_4^{\bullet-}$ generation (Kappler et al., 2014; Yuan et al., 2018). This finding was in accordance with previous reports, in which a Co_3O_4/reduced graphene oxide composite was demonstrated to be much more reactive than pure Co_3O_4 toward PMS activation for phenol degradation (Yao et al., 2012).

3.4. Influential factors on the catalytic activity of Co_3O_4-BC

This study further examined the effects of the amount of Co_3O_4 load in the composite, Co_3O_4-BC amount, PMS dose, solution pH and Cl^- concentration on the performance of the Co_3O_4-BC/PMS system. Fig. 4(a) shows that CAP degradation was slightly inhibited at a low Co_3O_4 loading (5 wt%), possibly because of less catalytic active sites for PMS activation to generate $SO_4^{\bullet-}$. An increase in the Co_3O_4 loading amount resulted in accelerated CAP degradation. As mentioned above, Co_3O_4, as the main active species in Co_3O_4-BC played a crucial role in the PMS activation process; thus, more Co_3O_4 provided extra active sites and enhanced the catalytic activity for PMS activation. However, further increasing the Co_3O_4 loading amount had a negligible effect on the final removal level of CAP with 97.6 ± 1.2% and 96.8 ± 0.1% for the 10 wt% and 20 wt% Co_3O_4 loading amounts, respectively. Generally, high nanoparticles loading will induce Co_3O_4 aggregation, which may not be beneficial for the catalytic activity of Co_3O_4-BC. In addition, the greater loading of Co_3O_4 on BC may reduce the surface area of the catalyst. Similarly, the degradation efficiency of CAP increased with increasing Co_3O_4-BC composite amount (Fig. 4(b)). However, when the composite amount further increased to 0.8 g/L, the removal percentage declined from 95.4 ± 3.0% to 84.6 ± 2.1%, which may be explained by the excess catalyst causing ineffective PMS consumption (Guan et al., 2013). This finding was consistent with our previous study, in which the amount of $MnFe_2O_4$ affected the generation efficiency of $SO_4^{\bullet-}$ in the $MnFe_2O_4$/PMS system and a further rise in the amount of $MnFe_2O_4$ adversely influenced $SO_4^{\bullet-}$ generation (Xu et al., 2019). These results indicated that the optimal Co_3O_4 loading amount on BC and the optimal Co_3O_4-BC composite amount were 10 wt% and 0.2 g/L, respectively.

It was obvious that CAP degradation rates increased remarkably with increasing PMS dose, probably due to the accelerated $SO_4^{\bullet-}$ generation at a high PMS dose (Fig. 4(c)). The removal percentage of CAP also increased from 49.3 ± 3.4% to 97.6 ± 1.2% as the PMS dose increased from 2 mM to 10 mM. However, at a higher PMS dose (15 mM), the CAP removal percentage exhibited a negligible increase, which might be attributed to the $SO_4^{\bullet-}$ scavenging effect caused by excess PMS (Gong et al., 2018).

Generally, the solution pH affects the degradation performance because it greatly affects the radical generation process and the speciation of contaminants. Fig. 4(d) shows that CAP degradation was significantly inhibited under alkaline conditions, with k_{app} declining from 0.3361 min^{-1} to 0.1273 and 0.0896 min^{-1} as the pH

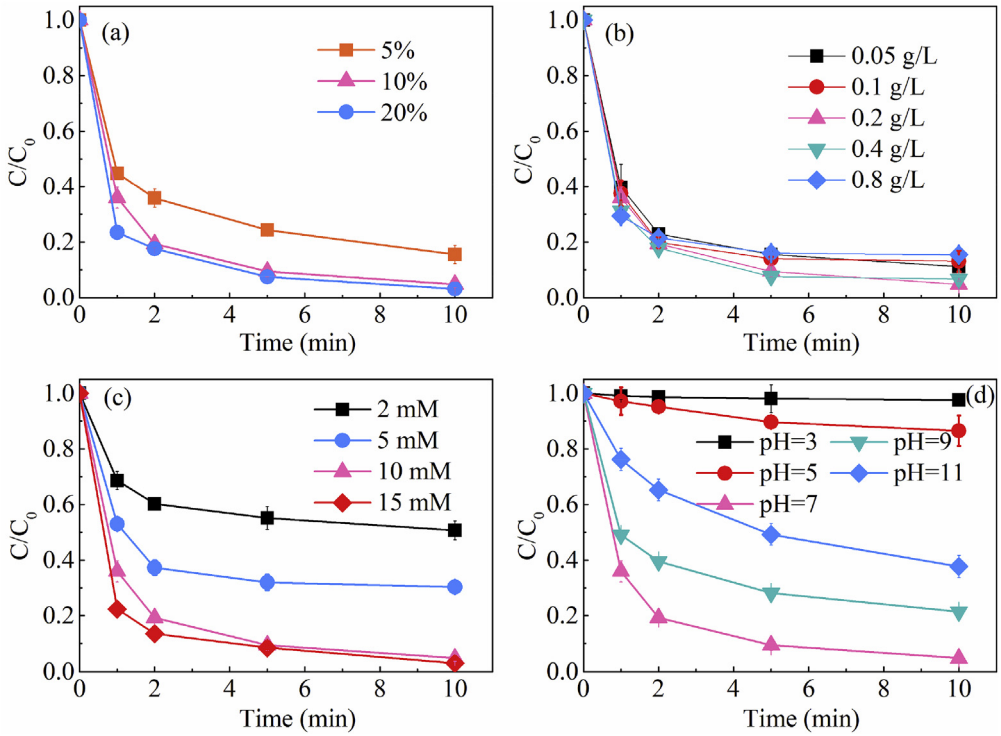

Fig. 4. Effects of the Co_3O_4 loading amount on BC (a), Co_3O_4-BC composite amount (b), PMS dose (c) and pH (d) on CAP degradation in the Co_3O_4-BC/PMS system. Experimental conditions: [CAP] = 30 mg/L [PMS] = 10 mM, [Co_3O_4-BC] = 0.2 g/L, pH = 7.0 for (a); [PMS] = 10 mM, pH = 7.0 for (b); [Co_3O_4-BC] = 0.2 g/L, pH = 7.0 for (c); [PMS] = 10 mM, [Co_3O_4-BC] = 0.2 g/L for (d).

value increased from 7 to 9 and 11, respectively. It has been reported that under alkaline conditions, a large amount of OH• is generated and plays a primary role in the degradation process (Nie et al., 2019). As mentioned above, the standard reduction potential of OH• is lower than that of $SO_4^{\bullet-}$. This difference may explain the decrease in CAP degradation under alkaline conditions. This finding was consistent with previous reports, in which $SO_4^{\bullet-}$ generation became difficult in a MnO_2/PMS system under alkaline conditions (Eslami et al., 2018). However, CAP degradation nearly ceased as the pH value decreased from 7 to 3, possibly because H_2SO_5 is the main form of PMS under acidic pH conditions, according to the pK_a value of PMS (pK_a = 9.4), and this species would obstruct the $SO_4^{\bullet-}$ generation process (Gong et al., 2018).

Additionally, Cl^- is considered a rate-limiting factor in $SO_4^{\bullet-}$-based processes due to its scavenging effect (Ghanbari and Moradi, 2017). Therefore, the effects of the Cl^- concentration on CAP degradation were also investigated, as shown in Fig. S9. The degradation efficiency of CAP decreased slightly with increasing Cl^- concentration within the range of 5–15 g/L, possibly because BC can adsorb Cl^- and reduce its scavenging effect (Dai et al., 2014). Furthermore, Co cation modified BC is a good anionic adsorbent for Cl^- (Novais et al., 2018). However, the removal percentage of CAP decreased to 79.2 ± 1.5% when the Cl^- concentration was further increased to 20 g/L, which may be explained by the high concentration of Cl^- exceeding the adsorption capacity of BC.

3.5. Mechanism of the Co_3O_4-BC/PMS system for CAP degradation

$SO_4^{\bullet-}$ and OH• are usually regarded as the main reactive radicals for contaminant oxidation in PMS activation. To determine the possible radicals present in the Co_3O_4-BC/PMS system, scavenging experiments were performed using MeOH and TBA as radical scavengers. MeOH can quench both $SO_4^{\bullet-}$ and OH• ($k_{SO4^{\bullet-}} = 1.6–7.7 \times 10^7\ M^{-1}\ s^{-1}$ and $k_{OH^{\bullet}} = 9.7 \times 10^8\ M^{-1}\ s^{-1}$), while TBA is an effective radical quencher for OH• only ($3.8–7.6 \times 10^8\ M^{-1}\ s^{-1}$) (Tang et al., 2018). According to the different reaction rate constants of the quenchers, the contributions of $SO_4^{\bullet-}$ and OH• to CAP degradation can be distinguished. As shown in Fig. 5, it can be clearly seen that both MeOH and TBA affected CAP degradation in the Co_3O_4-BC/PMS system. When 20 mM TBA was added to the system, CAP degradation was inhibited with the k_{app} decreasing from 0.3361 min^{-1} to 0.1154 min^{-1}. Moreover, further inhibition was observed (0.0687 min^{-1}) when the TBA concentration was increased to 100 mM. Compared with TBA, MeOH induced a more significant inhibition of CAP degradation with the k_{app} decreasing to 0.0381 min^{-1} (20 mM

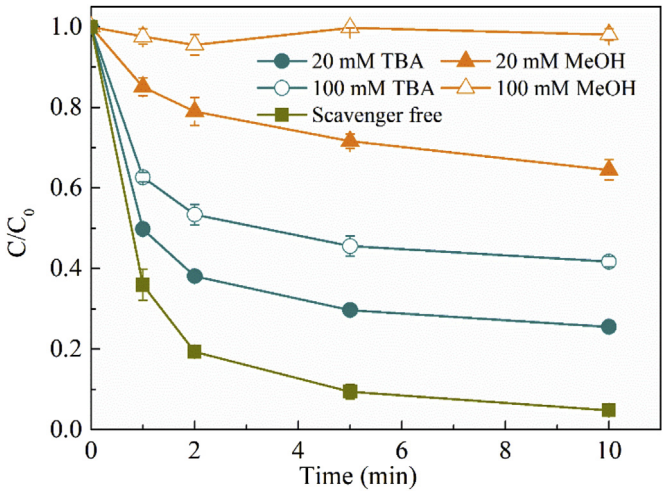

Fig. 5. Effect of methanol (MeOH) and tert-butanol (TBA) on the degradation of CAP in the Co_3O_4-BC/PMS system. Experimental conditions: [PMS] = 10 mM, [CAP] = 30 mg/L, [Co_3O_4-BC] = 0.2 g/L, pH = 7.0 (50 mM phosphate buffer).

MeOH), which was lower than the value observed with a similar concentration of TBA. CAP was hardly degraded (k_{app} = 0.0049 min^{-1}) in the presence of 100 mM MeOH, indicating that most of the free radicals were quenched.

The generated radicals were further confirmed by EPR with DMPO as a spin trap for radicals. A seven-line EPR spectrum was observed in the Co_3O_4-BC/PMS system (Fig. S10). This signal was assigned to DMPOX, which is an oxidized adduct formed through the oxidation of DMPO by free radicals (Fontmorin et al., 2016). As DMPO tends to be oxidized by radicals, the EPR signal might be ascribed to the oxidation capacity of $SO_4^{\bullet-}$ and OH• during the Co_3O_4-BC-mediated PMS activation process. In addition, the intensity of the DMPOX signal in the Co_3O_4-BC/PMS system was higher than that in the Co_3O_4/PMS system, indicating a higher concentration of free radicals, which further supported the finding that the Co_3O_4-BC/PMS system better induced CAP degradation. These results suggested that both $SO_4^{\bullet-}$ and OH• were produced and participated in the reaction, while $SO_4^{\bullet-}$ played a more dominant role than OH• in the degradation of CAP.

The mechanism of PMS activation by Co_3O_4-BC was illustrated as follows: (1) BC-Co^{2+} donates electrons that break the O-H and O-O bands of HSO_5^- and generate $SO_4^{\bullet-}$ (Eq. (2)); (2) BC-Co^{3+} is then reduced to BC-Co^{2+} by HSO_5^-, along with the production of $SO_5^{\bullet-}$ (Eq. (3)); (3) BC may activate HSO_5^- and generate $SO_5^{\bullet-}$ (Eq. (4)); and (4) OH• can be generated through the reaction of $SO_4^{\bullet-}$ with H_2O/OH^- (Eqs. (5) and (6)) (Bahrami et al., 2018). Here, BC plays a significant role in the electron transfer between the Co species and HSO_5^- and thus enhances the Co^{3+}/Co^{2+} redox cycle, which allowed the catalytic action of Co_3O_4-BC to work successively. It has already been proven that $SO_5^{\bullet-}$ (1.1 V) is a weaker radical species than $SO_4^{\bullet-}$ (2.5–3.1 V) and cannot effectively oxidize contaminants (Rodríguez-Chueca et al., 2017). This phenomenon may explain the poor degradation performance of CAP in the BC/PMS system.

$$\text{BC-Co}^{2+} + \text{HSO}_5^- \rightarrow \text{BC-Co}^{3+} + \text{SO}_4^{\bullet-} + \text{OH}^- \quad (2)$$

$$\text{BC-Co}^{3+} + \text{HSO}_5^- \rightarrow \text{BC-Co}^{2+} + \text{SO}_5^{\bullet-} + \text{H}^+ \quad (3)$$

$$\text{BC} + \text{HSO}_5^- \rightarrow \text{BC-H} + \text{SO}_5^{\bullet-} \quad (4)$$

$$\text{SO}_4^{\bullet-} + \text{H}_2\text{O} \rightarrow \text{SO}_4^{2-} + \text{OH}^{\bullet} + \text{H}^+ \quad (5)$$

$$\text{SO}_4^{\bullet-} + \text{OH}^- \rightarrow \text{SO}_4^{2-} + \text{OH}^{\bullet} \quad (6)$$

3.6. Reusability of Co_3O_4-BC

To evaluate the catalytic stability of Co_3O_4-BC, ten successive cycles of degradation were performed, as shown in Fig. 6. The Co_3O_4-BC/PMS system achieved effective CAP degradation with removal percentages of 97.8 ± 1.4% and 85.0 ± 1.5% in the 1st and 10th cycles, respectively, within 10 min. However, CAP degradation rate recovered gradually in the last consecutive runs, and further studies are still needed to optimize reusability of Co_3O_4-BC. Furthermore, another ten successive cycles of degradation were carried out and similar tendency was obtained. Based on the above results, it is clear that the Co_3O_4-BC composite has potential as a PMS activation catalyst for stable and long-term reuse.

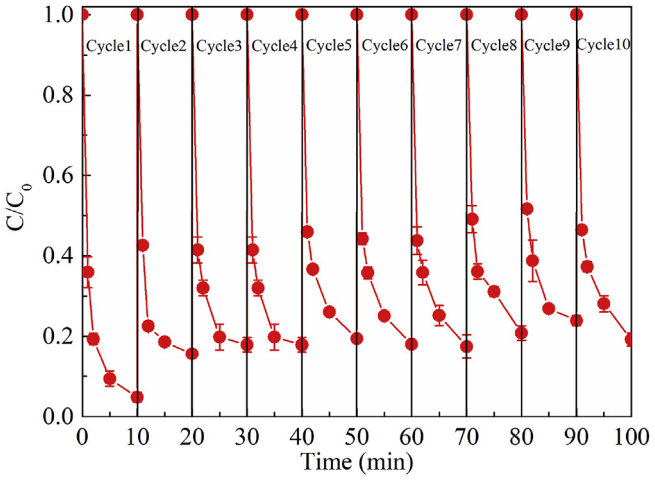

Fig. 6. Catalytic property of Co_3O_4-BC for cyclic use. Experimental conditions: [PMS] = 10 mM, [CAP] = 30 mg/L, [Co_3O_4-BC] = 0.2 g/L, pH = 7.0 (50 mM phosphate buffer).

4. Conclusions

In this study, an efficient catalyst, Co_3O_4-BC, was synthesized to activate PMS for chloramphenicols degradation. The active radical species were identified through radical quenching tests and ESR. The effects of Co_3O_4 loading on BC, Co_3O_4-BC amount, PMS doses and solution pH on antibiotics degradation were examined. The catalytic activity and stability of Co_3O_4-BC were also investigated. The major findings are summarized as follows:

(1) Co_3O_4-BC exhibited much better catalytic activity for PMS decomposition than Co_3O_4, thus resulting in superior degradation of CAP in the Co_3O_4-BC/PMS system, in which the apparent degradation rate constant was 5.1, 19.4 and 7.2 times that in the Co_3O_4/PMS, BC/PMS and PMS-alone systems, respectively. In addition, FF and TAP were also effectively degraded in the Co_3O_4-BC/PMS system at percentages of 86.4 ± 1.3% and 71.8 ± 1.0%, respectively. Furthermore, other organic compounds besides chloramphenicols may also be degraded in the Co_3O_4-BC/PMS system.

(2) The use of 10 wt% Co_3O_4 loading on BC, 0.2 g/L Co_3O_4-BC, 10 mM PMS and pH 7 yielded nearly complete removal of CAP with 10 min of reaction time. CAP degradation was considerably inhibited under extremely acidic or basic conditions. The removal efficiency of CAP slightly decreased when the Cl^- concentration increased to 20 g/L. Moreover, over 85.0 ± 1.5% of CAP was still removed in the 10th run, indicating that Co_3O_4-BC possessed good reusability and stability in long-term applications.

(3) Both $SO_4^{\bullet-}$ and OH• were produced in the Co_3O_4-BC/PMS system, and $SO_4^{\bullet-}$ played a dominant role in CAP degradation. Conducting BC promoted electron transfer between the Co species and HSO_5^-, provided a large surface area for the dispersal of Co_3O_4 and accelerated the Co^{3+}/Co^{2+} redox cycle, leading to a synergistic effect on the catalytic activity.

Declaration of competing interest

The authors declare no competing financial interest.

Acknowledgement

This work was supported by the Natural Science Foundation of

China (No. 51908542, 91751112, 41573071), the Postdoctoral Science of China (Grant No. 2018M632735), the Open Fund of Jiangsu Key Laboratory of Anaerobic Biotechnology (Jiangnan University) (No. JKLAB201705), the Shandong Provincial Natural Science Foundation (No. JQ201608) and the Young Taishan Scholars Program (No. tsqn20161054) of Shandong Province.

Appendix A. Supplementary data

Supplementary data to this article can be found online at https://doi.org/10.1016/j.envpol.2019.113610.

References

Anipsitakis, G.P., Dionysiou, D.D., Gonzalez, M.A., 2006. Cobalt-mediated activation of peroxymonosulfate and sulfate radical attack on phenolic compounds. implications of chloride ions. Environ. Sci. Technol. 40 (3), 1000–1007.

Bahrami, H., Eslami, A., Nabizadeh, R., Mohseni-Bandpi, A., Asadi, A., Sillanpää, M., 2018. Degradation of trichloroethylene by sonophotolytic-activated persulfate processes: optimization using response surface methodology. J. Clean. Prod. 198, 1210–1218.

Bai, B., Arandiyan, H., Li, J., 2013. Comparison of the performance for oxidation of formaldehyde on nano-Co_3O_4, 2D-Co_3O_4, and 3D-Co_3O_4 catalysts. Appl. Catal. B Environ. 142–143, 677–683.

Butler, M.S., Blaskovich, M.A., Cooper, M.A., 2016. Antibiotics in the clinical pipeline at the end of 2015. J. Antibiot. 70 (1), 3.

Chen, X., Chen, J., Qiao, X., Wang, D., Cai, X., 2008. Performance of nano-Co_3O_4/peroxymonosulfate system: kinetics and mechanism study using Acid Orange 7 as a model compound. Appl. Catal. B Environ. 80 (1–2), 116–121.

Dai, L., Wu, B., Tan, F., He, M., Wang, W., Qin, H., Tang, X., Zhu, Q., Pan, K., Hu, Q., 2014. Engineered hydrochar composites for phosphorus removal/recovery: lanthanum doped hydrochar prepared by hydrothermal carbonization of lanthanum pretreated rice straw. Bioresour. Technol. 161, 327–332.

Deng, D., Deng, F., Tang, B., Zhang, J., Liu, J., 2017a. Electrocatalytic reduction of low-concentration thiamphenicol and florfenicol in wastewater with multi-walled carbon nanotubes modified electrode. J. Hazard. Mater. 332, 168.

Deng, J., Feng, S., Zhang, K., Li, J., Wang, H., Zhang, T., Ma, X., 2017b. Heterogeneous activation of peroxymonosulfate using ordered mesoporous Co_3O_4 for the degradation of chloramphenicol at neutral pH. Chem. Eng. J. 308, 505–515.

Dong, H., Qiang, Z., Hu, J., Qu, J., 2017. Degradation of chloramphenicol by UV/chlorine treatment: kinetics, mechanism and enhanced formation of halonitromethanes. Water Res. 121, 178–185.

Du, J., Zhao, H., Wang, Y., Xie, H., Zhu, M., Chen, J., 2019. Presence and environmental risk assessment of selected antibiotics in coastal water adjacent to mariculture areas in the Bohai Sea. Ecotoxicol. Environ. Saf. 177, 117–123.

Eslami, A., Hashemi, M., Ghanbari, F., 2018. Degradation of 4-chlorophenol using catalyzed peroxymonosulfate with nano-MnO_2/UV irradiation: toxicity assessment and evaluation for industrial wastewater treatment. J. Clean. Prod. 195, 1389–1397.

Essandoh, M., Kunwar, B., Pittman, C.U., Mohan, D., Mlsna, T., 2015. Sorptive removal of salicylic acid and ibuprofen from aqueous solutions using pine wood fast pyrolysis biochar. Chem. Eng. J. 265, 219–227.

Feng, Y., Wu, D., Deng, Y., Zhang, T., Shih, K., 2016. Sulfate radical-mediated degradation of sulfadiazine by $CuFeO_2$ rhombohedral crystal-catalyzed peroxymonosulfate: synergistic effects and mechanisms. Environ. Sci. Technol. 50 (6), 3119–3127.

Fontmorin, J.M., Burgos Castillo, R.C., Tang, W.Z., Sillanpää, M., 2016. Stability of 5,5-dimethyl-1-pyrroline-N-oxide as a spin-trap for quantification of hydroxyl radicals in processes based on Fenton reaction. Water Res. 99, 24–32.

Ghanbari, F., Moradi, M., 2017. Application of peroxymonosulfate and its activation methods for degradation of environmental organic pollutants: Review. Chem. Eng. J. 310, 41–62.

Gong, Y., Zhao, X., Zhang, H., Yang, B., Xiao, K., Guo, T., Zhang, J., Shao, H., Wang, Y., Yu, G., 2018. MOF-derived nitrogen doped carbon modified g-C_3N_4 heterostructure composite with enhanced photocatalytic activity for bisphenol A degradation with peroxymonosulfate under visible light irradiation. Appl. Catal. B Environ. 233, 35–45.

Guan, Y.H., Ma, J., Ren, Y.M., Liu, Y.L., Xiao, J.Y., Lin, L.Q., Zhang, C., 2013. Efficient degradation of atrazine by magnetic porous copper ferrite catalyzed peroxymonosulfate oxidation via the formation of hydroxyl and sulfate radicals. Water Res. 47 (14), 5431–5438.

Guo, N., Wang, Y., Yan, L., Wang, X., Wang, M., Xu, H., Wang, S., 2017. Effect of bio-electrochemical system on the fate and proliferation of chloramphenicol resistance genes during the treatment of chloramphenicol wastewater. Water Res. 117, 95–101.

He, Z., Mansfeld, F., 2009. Exploring the use of electrochemical impedance spectroscopy (EIS) in microbial fuel cell studies. Energy Environ. Sci. 2 (2), 215–219.

Hu, P., Long, M., Bai, X., Wang, C., Cai, C., Fu, J., Zhou, B., Zhou, Y., 2017a. Monolithic cobalt-doped carbon aerogel for efficient catalytic activation of peroxymonosulfate in water. J. Hazard. Mater. 332, 195–204.

Hu, P., Su, H., Chen, Z., Yu, C., Li, Q., Zhou, B., Alvarez, P.J.J., Long, M., 2017b. Selective degradation of organic pollutants using an efficient metal-free catalyst derived from carbonized polypyrrole via peroxymonosulfate activation. Environ. Sci. Technol. 51 (19), 11288–11296.

Jiang, S.-F., Ling, L.-L., Chen, W.-J., Liu, W.-J., Li, D.-C., Jiang, H., 2019. High efficient removal of bisphenol A in a peroxymonosulfate/iron functionalized biochar system: mechanistic elucidation and quantification of the contributors. Chem. Eng. J. 359, 572–583.

Kappler, A., Wuestner, M.L., Ruecker, A., Harter, J., Halama, M., Behrens, S., 2014. Biochar as an electron shuttle between bacteria and Fe(III) minerals. Environ. Sci. Technol. Lett. 1 (8), 339–344.

Li, H., Shan, C., Pan, B., 2018. Fe(III)-doped g-C_3N_4 mediated peroxymonosulfate activation for selective degradation of phenolic compounds via high-valent iron-oxo species. Environ. Sci. Technol. 52 (4), 2197–2205.

Li, J., Shao, B., Shen, J., Wang, S., Wu, Y., 2013. Occurrence of chloramphenicol-resistance genes as environmental pollutants from awine feedlots. Environ. Sci. Technol. 47 (6), 2892–2897.

Li, Y., Li, Q., Zhou, K., Sun, X.L., Zhao, L.R., Zhang, Y.B., 2016. Occurrence and distribution of the environmental pollutant antibiotics in Gaoqiao mangrove area, China. Chemosphere 147, 25–35.

Liang, B., Cheng, H.Y., Kong, D.Y., Gao, S.H., Sun, F., Cui, D., Kong, F.Y., Zhou, A.J., Liu, W.Z., Ren, N.Q., 2013. Accelerated reduction of chlorinated nitroaromatic antibiotic chloramphenicol by biocathode. Environ. Sci. Technol. 47 (10), 5353–5361.

Luo, S., Wei, Z., Dionysiou, D.D., Spinney, R., Hu, W.-P., Chai, L., Yang, Z., Ye, T., Xiao, R., 2017. Mechanistic insight into reactivity of sulfate radical with aromatic contaminants through single-electron transfer pathway. Chem. Eng. J. 327, 1056–1065.

Mahdi-Ahmed, M., Chiron, S., 2014. Ciprofloxacin oxidation by UV-C activated peroxymonosulfate in wastewater. J. Hazard. Mater. 265, 41–46.

Nie, W., Mao, Q., Ding, Y., Hu, Y., Tang, H., 2019. Highly efficient catalysis of chalcopyrite with surface bonded ferrous species for activation of peroxymonosulfate toward degradation of bisphenol A: a mechanism study. J. Hazard. Mater. 364, 59–68.

Novais, S.V., Zenero, M.D.O., Barreto, M.S.C., Montes, C.R., Cerri, C.E.P., 2018. Phosphorus removal from eutrophic water using modified biochar. Sci. Total. Environ. 633, 825–835.

Qi, C.D., Yu, G., Huang, J., Wang, B., Wang, Y.J., Deng, S.B., 2018. Activation of persulfate by modified drinking water treatment residuals for sulfamethoxazole degradation. Chem. Eng. J. 353, 490–498.

Rodríguez-Chueca, J., Moreira, S.I., Lucas, M.S., Fernandes, J.R., Tavares, P.B., Sampaio, A., Peres, J.A., 2017. Disinfection of simulated and real winery wastewater using sulphate radicals: peroxymonosulphate/transition metal/UV-A LED oxidation. J. Clean. Prod. 149, 805–817.

Tang, L., Liu, Y., Wang, J., Zeng, G., Deng, Y., Dong, H., Feng, H., Wang, J., Peng, B., 2018. Enhanced activation process of persulfate by mesoporous carbon for degradation of aqueous organic pollutants: electron transfer mechanism. Appl. Catal. B Environ. 231, 1–10.

Wang, S., Wang, J., 2019. Activation of peroxymonosulfate by sludge-derived biochar for the degradation of triclosan in water and wastewater. Chem. Eng. J. 356, 350–358.

Xie, R., Ji, J., Huang, H., Lei, D., Fang, R., Shu, Y., Zhan, Y., Guo, K., Leung, D.Y.C., 2018. Heterogeneous activation of peroxymonosulfate over monodispersed Co_3O_4/activated carbon for efficient degradation of gaseous toluene. Chem. Eng. J. 341, 383–391.

Xu, H., Quan, X., Chen, L., 2019. A novel combination of bioelectrochemical system with peroxymonosulfate oxidation for enhanced azo dye degradation and $MnFe_2O_4$ catalyst regeneration. Chemosphere 217, 800–807.

Yan, J., Han, L., Gao, W., Xue, S., Chen, M., 2015. Biochar supported nanoscale zerovalent iron composite used as persulfate activator for removing trichloroethylene. Bioresour. Technol. 175, 269–274.

Yang, Q., Choi, H., Chen, Y., Dionysiou, D.D., 2008. Heterogeneous activation of peroxymonosulfate by supported cobalt catalysts for the degradation of 2,4-dichlorophenol in water: the effect of support, cobalt precursor, and UV radiation. Appl. Catal. B Environ. 77 (3–4), 300–307.

Yang, X., Chen, Z., Fang, J., Yang, Q., Zhao, W., Qian, X., Zhou, D., Liu, C., Chen, M., 2019. Freestanding 3D MoS_2 nanosheets/graphene aerogel heterostructure as a recyclable photocatalyst for efficiently degrading antibiotic residues. Mater. Lett. 252, 5–7.

Yang, Y., Banerjee, G., Brudvig, G.W., Kim, J.-H., Pignatello, J.J., 2018. Oxidation of organic compounds in water by unactivated peroxymonosulfate. Environ. Sci. Technol. 52 (10), 5911–5919.

Yao, Y., Yang, Z., Sun, H., Wang, S., 2012. Hydrothermal synthesis of Co_3O_4-graphene for heterogeneous activation of peroxymonosulfate for decomposition of phenol. Ind. Eng. Chem. Res. 51 (46), 14958–14965.

Yuan, J.H., Xu, R.K., Zhang, H., 2011. The forms of alkalis in the biochar produced from crop residues at different temperatures. Bioresour. Technol. 102 (3), 3488–3497.

Yuan, R., Hu, L., Yu, P., Wang, H., Wang, Z., Fang, J., 2018. Nanostructured Co_3O_4 grown on nickel foam: an efficient and readily recyclable 3D catalyst for heterogeneous peroxymonosulfate activation. Chemosphere 198, 204–215.

Zhang, B.G., Cheng, Y., Shi, J., Xing, X., Zhu, Y., Xu, N., Xia, J., Borthwick, A.G.L., 2019. Insights into interactions between vanadium (V) bio-reduction and pentachlorophenol dechlorination in synthetic groundwater. Chem. Eng. J. 375, 121965.